Rheol Acta (2015) 54:53–67
DOI 10.1007/s00397-014-0813-z

ORIGINAL CONTRIBUTION

Nonlinear viscoelasticity of complex fluids: A kinetic network model

Octavio Manero · Jorge E. Puig · Fernando Bautista · J. Paulo Garcia-Sandoval

Received: 9 May 2014 / Revised: 21 September 2014 / Accepted: 16 October 2014 / Published online: 23 November 2014

Abstract In this work, the rheological behavior of complex fluids is analyzed with a model based on the classical transient network formulation, in which the description of nonlinear viscoelasticity and time-dependent phenomena considers spatial and temporal variations of the entanglement density in the flow region. The entropic law of the segments that join entanglement points of macromolecules (or dispersed phase) is modeled with a Warner spring law with variable extensibility. The structure modification is described with a function that is dependent of a kinetic process that involves the formation of a more entangled microstate on one extreme, and a flow-induced degradation of the transient network with variable entanglement density on the other extreme (disentangled microstate). Predictions of the model under simple shear, inception of shear flow, stress relaxation, interrupted shear, and shear-thickening are compared with those of other models and with experiments.

Keywords Transient network · Complex fluids · Kinetic process · Nonlinear viscoelasticity

Financial support from project CONACYT-219810

O. Manero
Instituto de Investigaciones en Materiales,
Universidad Nacional Autónoma de México Ciudad
Universitaria, México D. F., 04510, México
e-mail: manero@unam.mx

J. E. Puig · F. Bautista · J. P. Garcia-Sandoval (✉)
Departamentos de Ingeniería Química y Física,
Universidad de Guadalajara, Blvd. M. García Barragán
1451, 44430, Guadalajara, México
e-mail: paulo.garcia@cucei.udg.mx

Introduction

In a previous publication (Rincón et al. 2005), the dynamics of rheologically complex fluids was analyzed with a model that considers two coupled kinetic processes, in which the presence of various entanglement scenarios is provided by the assumption of five microstates, representing increasing interactions among the macromolecules or dispersed phase. A complex kinetic system of coupled differential equations describes the evolution of the microstates. The segments entropic law is modeled with a Warner spring law (Warner 1972) with variable extensibility, which is a function of the kinetics of the microstates. The rheological functions are calculated according to the classical description of the transient network formulation, in which the pre-averaged approximation for the moments of the distribution function (Bird et al. 1987) is used.

It is important to mention that extensibility means here the maximum segment length, i.e., the critical length above which rupture of nodes occurs. In Rincón et al.'s model (2005), the extensibility is not a constant but a variable resulting from a kinetic process describing the dynamics of various microstates. Variable extensibility has also been considered in dumbbell models for dilute polymer solutions (Chilcott and Rallison 1988). These microstates reflect the complexity of interactions among the polymer molecules in suspension, which can be free chains or pendant chains of the network, on one extreme, or the many-node interactions available in a dense network, on the other extreme.

As in the classical description of a transient network (Lodge 1956; Green and Tobolsky 1946; Yamamoto 1958; Vaccaro and Marrucci 2000), the creation and destruction of nodes in the network considers that the creation is a thermally activated process while the destruction of nodes is due to the flow force, represented in Rincón et al. (2005) by the

viscous dissipation that drives the system into a less entangled network. The destruction mechanism in this model is represented by a function that has the same analytical form of the Warner expression with variable extensibility. Variation in the number of nodes is calculated by defining an average dynamic distance between nodes, which represents the maximum elongation of the chains undergoing deformation. The distance between nodes is calculated as an average of the five basic microstates, which represent all the possible structures in the network. The set of nonlinear coupled differential equations describing the evolution of the microstates is a complex system that provides a detailed description of the time-dependent concentration of each microstate.

In this work, a simplified expression of the kinetics of the microstates is provided, leading to a global scheme instead of a detailed kinetics of the evolution of each microstate. The drawback is that the global dissipation of the system is smaller than that calculated using the detailed description of the kinetics. On the other hand, this new description provides with a comparison to other more phenomenological models as special cases, but which have been tested and compared with ample experimental work. As it will be shown, if the extensibility of the segments is very large, the Warner force reduces to a linear spring force, and for a simple stoichiometry, the model proposed here reduces to the BMP model, which has been tested and compared extensively with experimental data in micellar and associative polymer systems (Soltero et al. 1999; Bautista et al. 2000, 2002; Manero et al. 2002; Caram et al. 2006).

Rincón et al.'s model (2005) revisited

In this approach, five microstates represent the possible configurations of the entire network. In the suggested form of representation, ω is ascribed to the specific microstate and the subindex represents the number of nodes that define the microstate. For example, ω_0 represents a pendant (dangling end) or a free chain with no nearby interactions, as in a dilute system. ω_1 represents a configuration with one node (crosslink) and two chains. Similarly, three extra configurations are proposed, representing a more packed state with two, three, and four nodes.

The next step is the calculation of the average properties of the network considering these five microstates. Under a given deformation or flow, some microstates are favored, depending on the properties of the system represented by the network and also on the characteristics of the deformation process.

In terms of average quantities, let us define, the maximum length of one extended free chain L_p, and the maximum end-to-end distance between nodes in the network (segments) including the dangling ends, $l'(t)$. By conservation of chains, the following relation arises:

$$\left(l'(t)\right)(\text{Number of segments}) = (\text{Number of chains})\left(L_p\right) \tag{1}$$

The total length of the chains is the product of the length of one free chain multiplied by the number of chains. The number of chains is the product of the concentration of chains (C) in every microstate times the occupied volume of the chains (V). Similarly, the number of segments in the network is the product of the occupied volume times the concentration of segments in every microstate, including the dangling ends. Table 1 shows the geometry of each microstate and the number of nodes, segments, and chains of each configuration. The number of chains is just the sum of products of the number concentration of chains and a weighted factor in every microstate. Thus, the number of segments is the sum of products of segment concentrations and weighted factors in every microstate. Equation 1 may be written in terms of the nondimensional distance between nodes, $l(t)$:

$$l(t) = \frac{l'(t)}{L_p} = \frac{C_0 + 2C_1 + 3C_2 + 3C_3 + 4C_4}{C_0 + 4C_1 + 7C_2 + 9C_3 + 12C_4} \tag{2}$$

The numerator of Eq. 2 represents the number concentration of chains of each microstate, whereas the denominator contains the number concentration of segments of every microstate (see Table 1). In addition, the nondimensional average distance between nodes for every microstate is shown in Table 1. The limits of $l(t)$ correspond to the situation where all chains are free, $l(t) = 1$, and that where all chains are in specific configurations. The nondimensional distance between nodes is then $m/(m + 2n)$ where m is the number of chains, n is the number of nodes, and $m + 2n$ is the number of segments.

Kinetic equations

Let us consider the following microstates kinetics (Weston and Schwarz 1972):

$$\omega_{1,0} \rightleftharpoons \omega_{1,n} \quad n = 1, 2, \ldots \tag{3}$$

$$2\omega_{1,0} \rightleftharpoons \omega_{2,n} \quad n = 1, 2, \ldots \tag{4}$$

$$\omega_{1,n_1} + \omega_{2,n_2} \rightleftharpoons \omega_{3,n} \quad n, n_1, n_2 = 1, 2, \ldots \tag{5}$$

$$\vdots$$

$$\sum_{i=1}^{\infty}\sum_{j=1}^{\infty} w_j \omega_{i,n_j} \rightleftharpoons \omega_{m,n} \quad m, n, n_j = 1, 2, \ldots \tag{6}$$

where $\omega_{i,j}$ is the microstate with i chains and j nodes. Equation 3 indicates that a single chain may have formed n entanglements with itself. Equation 4 represents that two

Table 1 Geometry and number of nodes, segments, and chains of several microstate configurations

Microstate		Geometry	Number of			$l(t)$
Present work	Rincón et. al		Chains	Nodes	Segments	
$\omega_{1,0}$	ω_0		1	0	1	1
$\omega_{1,1}$	–		1	1	3	$\frac{1}{3}$
$\omega_{2,1}$	ω_1		2	1	4	$\frac{2}{4}=\frac{1}{2}$
$\omega_{1,2}$	–		1	2	5	$\frac{1}{5}$
$\omega_{2,2}$	–		2	2	6	$\frac{2}{6}=\frac{1}{3}$
$\omega_{3,2}$	ω_2		3	2	7	$\frac{3}{7}$
$\omega_{1,3}$	–		1	3	7	$\frac{1}{7}$
$\omega_{2,3}$	–		2	3	8	$\frac{2}{8}=\frac{1}{4}$
$\omega_{3,3}$	ω_3		3	3	9	$\frac{3}{9}=\frac{1}{3}$
$\omega_{4,3}$	–		4	3	10	$\frac{4}{10}=\frac{1}{5}$
$\omega_{4,4}$	ω_4		4	4	12	$\frac{4}{12}=\frac{1}{3}$
$\omega_{m,n}$	–		m	n	$m+2n$	$\frac{m}{m+2n}$

free chains form a structure with n nodes, while Eq. 5 indicates that a free chain with n_1 nodes and two chains with n_2 nodes form a new structure with three chains and n nodes. Following this procedure, Eq. 6 describes the general case in which a number of structures with various chains and nodes combine to form a new structure with m chains and n nodes. If we now consider two dominant species, namely, $\omega_{1,0}$ and $\omega_{m,n}$, these equations may be simplified by making the summation of the above kinetics, to give:

$$m\omega_{1,0} \rightleftharpoons \omega_{m,n} \tag{7}$$

where $1 \leq m \leq n$. Furthermore, according to the mass action law, we assume that the kinetics for node formation is $k_1 C_0^P$, where C_0 is the concentration of species $\omega_{1,0}$ and p ($\leq m$) accounts for the combined effect of formation of nodes within the same chain or structure formation among several chains. The kinetics for nodes destruction is represented by the term $k_2 C_n$, where C_n is the concentration of species $\omega_{m,n}$. n is in this case the average number of nodes for the polymer in the quiescent state, which is correlated with the chemical composition of the chains, their length, and solvent type. Accordingly, the overall kinetics may be expressed as:

$$\frac{dC_0}{dt} = -k_1 C_0^p + mk_2 C_n \tag{8}$$

$$\frac{dC_n}{dt} = \frac{1}{m} k_1 C_0^p - k_2 C_n \tag{9}$$

here, C_0 and C_n are the concentrations of free wormlike and entangled chains, respectively, and k_1 and k_2 are the forward

and backward kinetic constants, respectively. The forward reaction induces the formation of a more complex configuration (i.e., that with a larger number of chains and nodes) and the reverse reaction gives rise to a configuration with smaller number of chains and nodes. The forward process is thermally activated, whereas the reverse process depends on the viscous dissipation.

As stated above, the extensibility of the microstates may be defined as the ratio of the number of chains and number of segments, i.e.,

$$l = \frac{C_0 + mC_n}{C_0 + (m+2n)\,C_n} \tag{10}$$

The limits of Eq. 10 depend on the strength of the flow: when the flow strength is high, the dominant microstate is $\omega_{1,0}$, and hence C_0 is large. In this case, the extensibility tends to unity. On the contrary, if the flow strength is low, the dominant microstate is $\omega_{m,n}$, and therefore C_n is now large. In the latter case, the extensibility tends to $m/(m+2n)$.

The density distribution function

Let $\psi_0\left(\underline{r}, \underline{Q}, t\right)$ and $\psi_n\left(\underline{r}, \underline{Q}, t\right)$ represent the number density distribution of free chains and entangled chains in space, configuration space, and time, respectively. The equations governing the configuration density function $\psi\left(\underline{r}, t\right)$ follows the above kinetics through Eqs. 7, 8, and 9 as follows (Bird et al. 1987; Bhave et al. 1991; Beris and Mavrantzas 1994):

$$\begin{aligned}\frac{\partial \psi_0}{\partial t} &+ \nabla_{\underline{r}} \cdot \dot{\underline{r}}\psi_0 - \frac{k_B T}{2\varsigma_0}\nabla^2_{\underline{r}}\psi_0 + \nabla_{\underline{Q}} \cdot \left(\underline{Q} \cdot \nabla \dot{\underline{r}}\right)\psi_0 \\ &- \frac{2k_B T}{\varsigma_0}\nabla^2_{\underline{Q}}\psi_0 + \frac{2H_0}{\varsigma_0}\nabla_{\underline{Q}} \cdot \psi_0 = -k_1\psi_0^p + mk_2\psi_n \end{aligned} \tag{11}$$

$$\begin{aligned}\frac{\partial \psi_n}{\partial t} &+ \nabla_{\underline{r}} \cdot \dot{\underline{r}}\psi_n - \frac{k_B T}{2\varsigma_n}\nabla^2_{\underline{r}}\psi_n + \nabla_{\underline{Q}} \cdot \left(\underline{Q} \cdot \nabla \dot{\underline{r}}\right)\psi_n \\ &- \frac{2k_B T}{\varsigma_n}\nabla^2_{\underline{Q}}\psi_n + \frac{2H_n}{\varsigma_n}\nabla_{\underline{Q}} \cdot \psi_n = \frac{1}{m}k_1\psi_0^p - k_2\psi_n \end{aligned} \tag{12}$$

The subscripts 0 and n denote free chains and entangled chains, respectively. The drag coefficient ς is assumed constant and H is the spring constant. k_B is the Boltzmann constant, T the temperature, $\dot{\underline{r}}$ the rate of change of the end-to-end vector $\underline{r}$ in physical space, and $\underline{Q}$ the vector joining the extremes of a free wormlike chain, but in the case of entangled chains, it refers to the vector joining two nodes. The concentrations of free and entangled chains are:

$$C_0\left(\underline{r}, t\right) = \int \psi_0\left(\underline{r}, t\right) d\underline{Q} \tag{13}$$

$$C_n\left(\underline{r}, t\right) = \int \psi_n\left(\underline{r}, t\right) d\underline{Q} \tag{14}$$

The conservation equation for the segment density within the specific kinetics is obtained upon integration (in the configuration space) of Eqs. 11 and 12:

$$\frac{dC_0}{dt} + \nabla \cdot \underline{J}_0 = -k_1 C_0^p + mk_2 C_n \tag{15}$$

$$\frac{dC_n}{dt} + \nabla \cdot \underline{J}_n = \frac{1}{m}k_1 C_0^p - k_2 C_n \tag{16}$$

where the mass flux vector of each species is given by:

$$\underline{J}_0 = -D_0 \nabla C_0 - \frac{H_0}{\varsigma_0}\nabla \cdot \left\langle \underline{QQ} \right\rangle_0 \tag{17}$$

$$\underline{J}_n = -D_n \nabla C_n - \frac{H_n}{\varsigma_n}\nabla \cdot \left\langle \underline{QQ} \right\rangle_n \tag{18}$$

In Eqs. 17 and 18, the diffusivity is $D = k_B T/\varsigma$ for free (D_0) and entangled (D_n) chains, respectively. The conformation tensors for free and entangled chains are $\left\langle \underline{QQ} \right\rangle_0 = \int \underline{QQ}\psi_0\left(\underline{r}, \underline{Q}, t\right) d\underline{Q}$ and $\left\langle \underline{QQ} \right\rangle_n = \int \underline{QQ}\psi_n\left(\underline{r}, \underline{Q}, t\right) d\underline{Q}$.

Substituting Eqs. 17 and 18 into Eqs. 15 and 16 gives:

$$\begin{aligned}\frac{dC_0}{dt} &= D_0\nabla^2 C_0 + \frac{1}{4\lambda_0}\left(\nabla \cdot \nabla \cdot \left\langle \underline{QQ} \right\rangle_0\right) - k_1 C_0^p \\ &+ mk_2 C_n \end{aligned} \tag{19}$$

$$\begin{aligned}\frac{dC_n}{dt} &= D_n\nabla^2 C_n + \frac{1}{4\lambda_n}\left(\nabla \cdot \nabla \cdot \left\langle \underline{QQ} \right\rangle_n\right) + \frac{1}{m}k_1 C_0^p \\ &- k_2 C_n \end{aligned} \tag{20}$$

where $\lambda_0 = \varsigma_0/4H_0$ and $\lambda_n = \varsigma_n/4H_n$ are the relaxation time constant for each species.

The equations for the moments of the distribution function, specifically, the second-moment equations, can be obtained by multiplying the distribution function equation by $\underline{QQ}$ and averaging over the configuration space, within the pre-averaged Peterlin approximation (Bird et al. 1987). The convected time derivative of $\underline{\underline{X}}$ is denoted by the symbol $\overset{\nabla}{\underline{\underline{X}}}$. The equations for the configuration tensor of the free chains and the entangled chains are given by Eqs. 21 and 22:

$$\begin{aligned}\overset{\nabla}{\left\langle \underline{QQ} \right\rangle}_0 &= -\frac{1}{\lambda_0}\left\langle \underline{QQ} \right\rangle_0 + 4C_0 D_0 \underline{\underline{I}} + D_0\nabla^2\left\langle \underline{QQ} \right\rangle_0 \\ &- k_{1p}\left\langle \underline{QQ} \right\rangle_0 + mk_2\left\langle \underline{QQ} \right\rangle_n \end{aligned} \tag{21}$$

$$\begin{aligned}\overset{\nabla}{\left\langle \underline{QQ} \right\rangle}_n &= -\frac{1}{\lambda_n}\left\langle \underline{QQ} \right\rangle_n + 4C_n D_n \underline{\underline{I}} + D_n\nabla^2\left\langle \underline{QQ} \right\rangle_n \\ &- k_2\left\langle \underline{QQ} \right\rangle_n + \frac{k_{1p}}{m}\left\langle \underline{QQ} \right\rangle_0 \end{aligned} \tag{22}$$

where $k_{1p} = k_1 C_0^{p-1}$. Here, we consider the case of nonlinear springs and the contribution to the total stress is given by

$$\underline{\underline{\tau}} = H_0\left\langle \underline{QQ} \right\rangle_0 + H_n\left\langle \underline{QQ} \right\rangle_n - (C_0 + C_n)\,kT\,\underline{\underline{I}} + \eta_s \underline{\underline{D}} \tag{23}$$

where the Warner expression for the spring force is:

$$\underline{F}(Q) = -H' \frac{\underline{Q}}{1 - \left(\underline{Q}/l(t)\right)^2} \tag{24}$$

and η_s is the solvent viscosity. Equations 19 to 24 are the main results of this section. In the following, particular cases are analyzed for specific problems.

No diffusion limit

In the absence of diffusion of the configuration tensors, and considering that the free chains relax in a time scale much shorter than those entangled, Eq. 21 may be solved for the configuration tensor of free chains to give:

$$\langle \underline{QQ} \rangle_0 = \frac{mk_2}{1/\lambda_0 + k_{1p}} \langle \underline{QQ} \rangle_n + \frac{4C_0 D_0}{1/\lambda_0 + k_{1p}} \underline{\underline{I}}$$

which upon substitution into Eq. 22 yields:

$$\begin{aligned} &\beta\left(k_{1p}, k_2, \lambda_0, \lambda_n\right) \langle \underline{QQ} \rangle_n + \overset{\triangledown}{\langle \underline{QQ} \rangle}_n \\ &= \left(4C_n D_n + \frac{4k_{1p} C_0 D_0}{m\left(1/\lambda_0 + k_{1p}\right)}\right) \underline{\underline{I}} \end{aligned} \tag{25}$$

where, similarly to transient network theories, the so-called destruction function β is given by:

$$\beta\left(k_{1p}, k_2, \lambda_0, \lambda_n\right) = \frac{1}{\lambda_n} \frac{1 + \lambda_n k_2 + \lambda_0 k_{1p}}{1 + \lambda_0 k_{1p}} \tag{26}$$

This function embodies the kinetic constants and the two relaxation times of the system, and possesses two asymptotic limits. When the destruction of nodes and chains predominate (high flow strength), $k_2 \gg k_{1p}$, hence

$$\beta\left(k_{1p}, k_2, \lambda_0, \lambda_n\right) = k_2 \tag{27}$$

In Eq. 27, the process is governed by the relaxation time of free chains. On the other hand, if the flow strength is low, the reformation of nodes predominates ($k_2 \ll k_{1p}$), and in this case, it gives:

$$\beta\left(k_{1p}, k_2, \lambda_0, \lambda_n\right) = \frac{1}{\lambda_n} \tag{28}$$

where the process is now governed by the relaxation time of the entangled chains. In this context, we can relate the processes of formation of chains and nodes to a thermally activated process, while their destruction by flow as a process undergoing dissipation.

The forward rate constant (k_1) is the structure-formation kinetic quantity that has an Arrhenius dependence with temperature (Manero et al. 2002), associated to a thermally activated process. The energy barrier is proportional to the energy change involved in the microstate transition, i.e., $k_1 \propto \exp\left(-E_0/KT\right)$. The reverse rate constant (k_2) times the dissipation function represents the breakage or modification process of the transient network at a given time t. Then, the reverse process is a function of the dissipation, i.e., $k_2 \propto \underline{\underline{\tau}} : \underline{\underline{D}}$, and hence, a function of the stress level (flow strength) and flow type through the velocity-gradient tensor. As the flow strength increases, one expects that the breakage process to overcome the reformation process, favoring microstates with low number of nodes. On the contrary, if the flow is weak, formation of more complex structures with larger number of chains and nodes is induced. Therefore:

$$k_1 = \kappa_1(T), \quad k_2 = \kappa_2 \underline{\underline{\tau}} : \underline{\underline{D}}$$

These relations justify the assumption used in network theories in which the destruction function depends on the configuration tensors through Eq. 25. In the absence of diffusion, the dynamics are dominated by the "reactions," and hence, Eqs. 15 and 16 become:

$$\frac{dC_0}{dt} = -k_1 C_0^p + mk_2 C_n \tag{29}$$

$$\frac{dC_n}{dt} = \frac{1}{m} k_1 C_0^p - k_2 C_n \tag{30}$$

To gather these equations into a single one, we define the total concentration of free and entangled chains as $C_c = C_0 + mC_n$. As far as the total concentration is constant, its time derivative is:

$$\frac{dC_c}{dt} = \frac{dC_0}{dt} + m\frac{dC_n}{dt} = 0$$

Defining $x = C_0/C_c$, as the fraction of free chains, then $1 - x = mC_n/C_c$ is the fraction of entangled chains, and hence Eq. 29 becomes:

$$\begin{aligned} \frac{dx}{dt} &= -k_1 C_c^{p-1} x^p + k_2 (1 - x) \\ &= -\kappa_1(T) C_c^{p-1} x^p + \kappa_2 (1 - x)\left(\underline{\underline{\tau}} : \underline{\underline{D}}\right) \end{aligned} \tag{31}$$

Linear springs

In this particular case, the equation for the force is linear, implying a very large extensibility (Hookean law). The constitutive equations for the stress of the entangled chains can be obtained by substituting the expression for the stress (32),

$$\underline{\underline{\tau}}_n = H_n \langle \underline{QQ} \rangle_n - C_n kT \underline{\underline{I}} \tag{32}$$

into Eq. 25. This gives:

$$\beta \underline{\underline{\tau}}_n + \overset{\triangledown}{\underline{\underline{\tau}}}_n = 2G_n \underline{\underline{D}} + G_n \left(\frac{1}{\lambda_n} - \beta + \frac{k_{1p}}{m\left(1 + \lambda_0 k_{1p}\right)}\right) \underline{\underline{I}} \tag{33}$$

where the elastic modulus is defined as

$$G_n = C_n kT \tag{34}$$

When the entanglements dominate, Eq. 33 becomes the upper-convected Maxwell equation within a small isotropic term.

Dividing each term of Eq. 33 by G_n, the variable β/G_n is just the fluidity. In fact, the asymptotic limits, Eqs. 27 and 28, can be defined in terms of the characteristic fluidities:

At small strain rates (low flow strength)

$$\beta/G_n = \frac{1}{\lambda_n G_n} = \varphi_0 \tag{35}$$

At large strain rates (high flow strength)

$$\beta/G_n = \frac{k_2}{G_n} = \varphi_\infty \tag{36}$$

Since $k_2 = O\,(1/\lambda_0)$ and $\lambda_n \gg \lambda_0$, the fluidity increases from φ_0 to φ_∞ as the strain rate increases, and in general

$$\beta/G_n = \varphi \tag{37}$$

A relation that complies with the above limits can be expressed as a first approximation in terms of a linear equation for the fluidity as a function of the characteristic fluidities of each microstate, i.e.:

$$\varphi = \varphi_\infty x + \varphi_0\,(1 - x) \tag{38}$$

The fluidity is then a function of the concentration fraction of free chains (x) and entangled chains ($1 - x$); each microstate having a characteristic fluidity. In fact, for weak flows, the concentration of entangled chains dominates and the fluidity is close to φ_0. In contrast, for strong flows, the fraction of free micelles increases and hence the fluidity of the system is close to φ_∞. This is in accord to the limits given in Eqs. 27 and 28.

In terms of the fluidities, Eq. 31 may be expressed as follows:

$$\frac{\partial \varphi}{\partial t} = -\frac{1}{\lambda}\,(\varphi - \varphi_0)^p + \kappa_2\,(\varphi_\infty - \varphi)\left(\underline{\underline{\tau}} : \underline{\underline{D}}\right) \tag{39}$$

where the characteristic time for structure formation is given by:

$$\lambda = \kappa_1^{-1}\,(T)\left(\frac{C_c}{\varphi_\infty - \varphi_0}\right)^{1-p}$$

Finally, the extensibility becomes

$$l = \frac{(\varphi - \varphi_0) + m\,(\varphi_\infty - \varphi)}{(\varphi - \varphi_0) + (m + 2n)\,(\varphi_\infty - \varphi)} \tag{40}$$

Under steady-state, Eq. 39 reveals that the normalized dissipation can be expressed as follows:

$$\left(\underline{\underline{\tau}} : \underline{\underline{D}}\right) = \frac{1}{\lambda\kappa_2}\frac{(\varphi - \varphi_0)^p}{\varphi_\infty - \varphi} \quad \varphi < \varphi_\infty \tag{41}$$

The numerator in Eq. 41 expresses increasing dissipation due to larger fluidity resulting from higher concentration of disentangled chains, whereas the denominator expresses decreasing concentration of entangled chains as the fluidity approaches φ_∞. This means that when the fluidity is small, the fluid structure is mostly preserved and hence the concentration of disentangled chains is small. At high deformation rates, structure modification is strong and the resulting large fluidity is associated to large concentration of disentangled chains.

Homogeneous simple shear flow

In homogeneous simple shear flow, the shear rate is constant (x is the flow direction and y is that of the velocity gradient), and therefore Eq. 25 leads to the following system of coupled differential equations for the components of the configuration tensor (after neglecting a small isotropic contribution):

$$\langle XX\rangle + \frac{1}{\beta}\left(\frac{d}{dt}\langle XX\rangle - 2\dot{\gamma}\,\langle XY\rangle\right) = \frac{4}{\beta}C_n D_n \tag{42}$$

$$\langle YY\rangle + \frac{1}{\beta}\left(\frac{d}{dt}\langle YY\rangle\right) = \frac{4}{\beta}C_n D_n \tag{43}$$

$$\langle ZZ\rangle + \frac{1}{\beta}\left(\frac{d}{dt}\langle ZZ\rangle\right) = \frac{4}{\beta}C_n D_n \tag{44}$$

$$\langle XY\rangle + \frac{1}{\beta}\left(\frac{d}{dt}\langle XY\rangle - \dot{\gamma}\,\langle YY\rangle\right) = 0 \tag{45}$$

The trace of the configuration tensor is the squared end-to-end distance of the segments:

$$\left\langle Q^2\right\rangle = \langle XX + YY + ZZ\rangle \tag{46}$$

The optical functions (birefringence and extinction angle) are given by:

$$\frac{\Delta n}{C} = \frac{1}{G_n}\sqrt{\langle XX - YY\rangle^2 + 4\,\langle XY\rangle^2} \tag{47}$$

where C is an optical constant related to the intrinsic polarizability of the micellar/solvent system. In addition, the orientation angle is given by

$$\chi = \frac{1}{2}\arctan\left[\frac{2\,\langle XY\rangle}{\langle XX - YY\rangle}\right] \tag{48}$$

The limits of the squared end-to-end distance of the segments in Eq. 46 lie in the interval $\left(\left\langle Q^2\right\rangle_{eq}\right) \le \left(\left\langle Q^2\right\rangle\right) \le \left(l\,(t)^2\right)$ and hence this range depends on the dynamics of the microstates and the extensibility represented by $l\,(t)$. The birefringence in Eq. 47 tends to the same asymptote of Eq. 46 at high shear rates, and therefore, its range lies within the limits $0 \le \Delta n \le l\,(t)^2$.

Under steady simple shear, the following expressions for the stress and normal stress differences are obtained (with

$\beta/G_n = \varphi$ and Warner force):

$$\frac{\tau_{xy}}{G_n} = \frac{1}{1 - Q^2/l\,(t)^2}\left(\frac{\dot{\gamma}}{G_n\varphi}\right) \tag{49}$$

$$\frac{N_1}{2G_n} = \frac{1}{1 - Q^2/l\,(t)^2}\left(\frac{\dot{\gamma}}{G_n\varphi}\right)^2 \tag{50}$$

$$N_2 = 0 \tag{51}$$

Moreover, the birefringence and extinction angle are given by:

$$\frac{\Delta n}{C} = 2\left(\frac{\dot{\gamma}}{G_n\varphi}\right)\sqrt{1 + \left(\frac{\dot{\gamma}}{G_n\varphi}\right)^2} \tag{52}$$

$$\chi = \frac{1}{2}\arctan\left[\left(\frac{\dot{\gamma}}{G_n\varphi}\right)^{-1}\right] \tag{53}$$

The orientation angle tends to 45° at low shear rates and decreases down to zero at high shear rates. However, the asymptotic behavior at high shear rates is dependent on the scaling of β with the extensibility $l\,(t)$.

Calculation procedure

For the kinetics described by Eq. 39 with the expression for the stress given by Eq. 49, we obtain for simple shear,

$$\frac{\partial\varphi}{\partial t} = -\frac{1}{\lambda}\,(\varphi - \varphi_0)^p + \kappa_2\,(\varphi_\infty - \varphi)\,\dot{\gamma}\left(\frac{G_0}{1 - Q^2/l\,(t)^2}\frac{\dot{\gamma}}{G_0\varphi}\right) \tag{54}$$

For the case of linear springs, Eq. 54 reduces to:

$$\frac{\partial\varphi}{\partial t} = -\frac{1}{\lambda}\,(\varphi - \varphi_0)^p + \kappa_2\,(\varphi_\infty - \varphi)\,\frac{\dot{\gamma}^2}{\varphi} \tag{55}$$

Given the material constants λ, k, φ_0, φ_∞, and G_0, for an applied shear-rate $\dot{\gamma}$, the expressions for l^2 and $\langle Q^2\rangle$ Eq. 40 and 46, respectively may be plugged into Eqs. 54 and 42–45 to solve for the fluidity φ and the components of the configuration tensor. Then, with the shear rate and the resulting fluidity, l^2 and $\langle Q^2\rangle$ may be readily calculated (provided $Q^2 < l^2$) and with these values the rheological functions Eqs. 49 to 53 are henceforth evaluated.

Model predictions

In this section, we present results for the cases of steady simple shear, inception of flow, stress relaxation, and interrupted shear.

Steady simple shear

In Fig. 1, the viscosity (Fig. 1a), normalized stress and stress difference (Fig. 1b), extensibility and end-to-end distance of the segments (Fig. 1c), and the birefringence and extinction angle (Fig. 1d) are plotted as a function of shear rate. The number of chains is two, one node, and kinetic order is one. The shear rate is normalized with the Maxwell relaxation time (β_0^{-1}) namely $\beta_0 = G_0\varphi_0$.

In Fig. 1a, the normalized viscosity decreases with shear rate exhibiting the first and the second Newtonian plateaus at small and high shear rates, respectively. Past a critical shear rate, a power-law region with slope near minus one is reached, approaching the second Newtonian plateau at high shear rates. For large enough shear rates, the rate of network degradation overcomes the rate of reformation and this leads to shear-thinning. In Fig. 1b, the normalized shear stress and the first normal stress difference are plotted against the nondimensional shear rate. At low shear rates, the stress and N_1 approach the limiting slopes of one and two (not shown), respectively. A monotonic increase as the shear rate augments is observed up to a region where a sudden increase is predicted in both functions. This behavior at high shear rates is due to the approach of the segments length to their maximum extensibility (according to Eq. 40; in this case, $l = 0.5$ at low shear rates and it approaches 1 at high shear rates) wherein in the nonlinear regime of deformation the force in the Warner expression increases steeply as $Q \to l$ (see Fig. 1c). The birefringence also increases monotonically, similar to the growth of the segments length. The extinction angle indicates the increasing alignment of the segments along the flow direction (see Fig. 1d).

It is interesting that the values predicted for the birefringence as a function of shear rate are different to those predicted for the stress. Values of the stress are larger than those of the birefringence, and the upturn of the stress is attained at lower values of the shear rate. The birefringence, in turn, presents a much gradual increase compared to that of the stress; the latter is more abrupt. This prediction reveals that substantial alignment of the segments occurs at shear rates higher than those implied in the stress growth.

In Fig. 2, the kinetic-order is changed from one to two, with same number of chains (2) and number of nodes (1). Steady-state results are similar to those shown in Fig. 1, except that the magnitudes are different in the high shear rate range. A stronger nodes reformation function results in a more entangled network. The nonlinear regime in the segment force in this case is attained at larger rate, revealing that in a more entangled network, the flow strength should be larger to disrupt the network, as seen in Fig. 2c. In turn, the stress and normal stress difference in the nonlinear regime corresponding to the observed abrupt growth as the shear rate increases (see Fig. 2b) and is predicted to occur

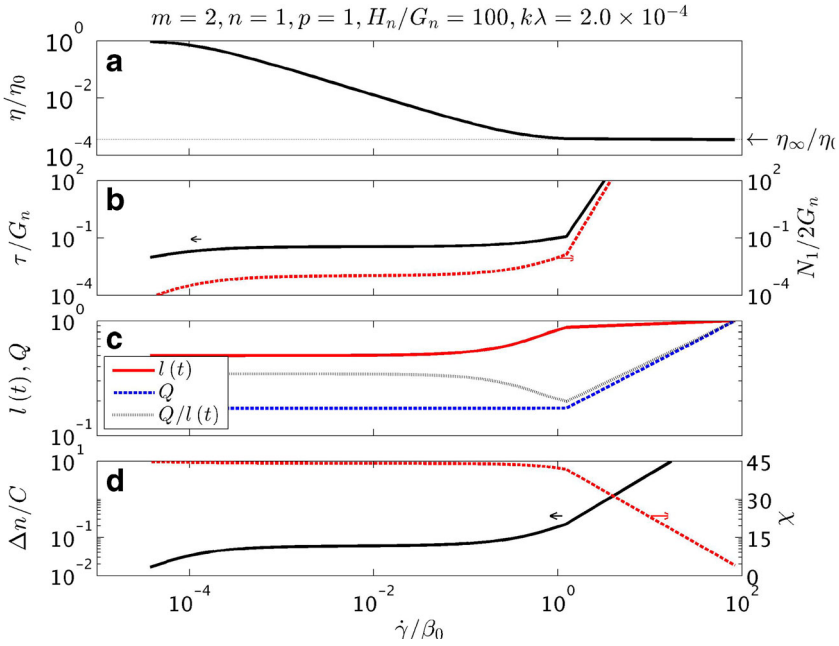

Fig. 1 System with two chains, one node and kinetic order 1, rheological functions with nondimensional shear rate. **a** Normalized viscosity; **b** normalized stress and first normal stress difference; **c** extensibility, end-to-end distance of the segments, and their ratio; and **d** birefringence and extinction angle

at larger shear rates when the kinetics order is 2. Consequently, the viscosity in Fig. 2a is slightly larger in the high shear rate region as compared with that shown in Fig. 1a for first-order kinetics. It is interesting that the birefringence in Fig. 2d reveals smaller degree of anisotropy at comparable shear rates in the second-order kinetics, again in agreement with the picture of delayed network disruption.

When the kinetics order is changed to 5, keeping the number of chains and nodes to 10 and 50, respectively, qualitatively different results are obtained. In this case, in the whole range of shear rates, the segments end-to-end distance is close to its maximum extensibility, fully inside the nonlinear regime. An interesting result is the variation of the viscosity with shear rate, shown in Fig. 3a. The curve depicts the two asymptotic regions at low and high shear rates, as before, but in between it describes two power-law regions, the one with a larger slope observed at high shear rates. It approaches the second Newtonian region with

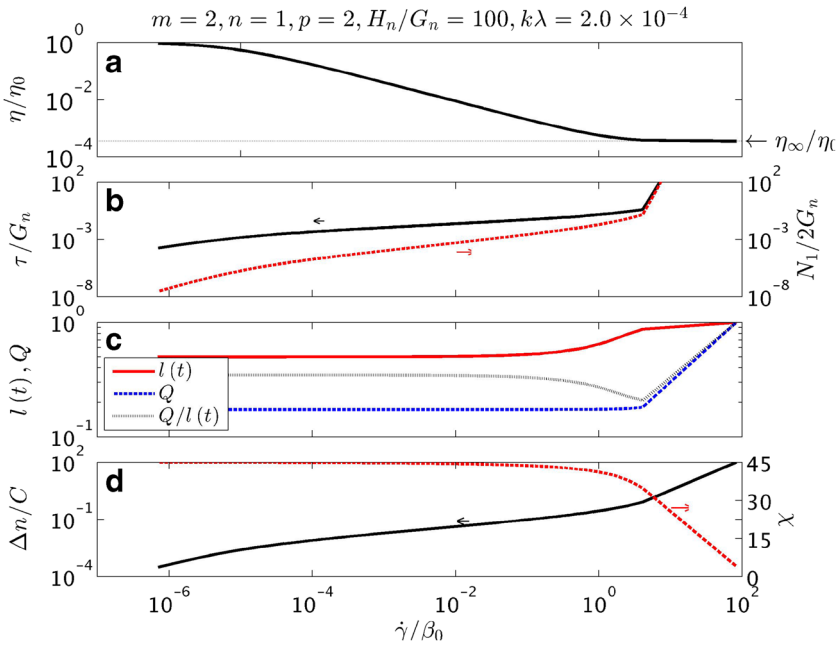

Fig. 2 Same as in Fig. 1 for a system with two chains, one node, and second-order kinetics

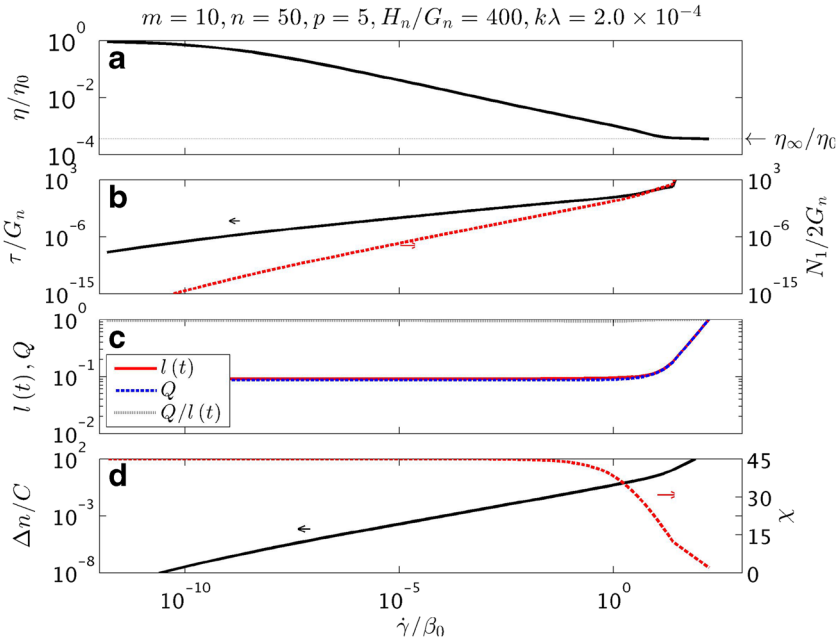

Fig. 3 Same as in Fig. 1 for a system with 10 chains, 50 nodes, and kinetic order 5

comparatively larger values than those of the previous cases. This highly nonlinear behavior results from the effect of high node reformation at low shear rates.

Predictions cover the range of very low shear rates just to find the asymptotic first Newtonian region. Of course, for real fluid behavior, this asymptotic region is not observed. Instead, at very low shear rates, the stress in this case would attain an almost flat value (the yield stress), as observed in Fig. 3b. These predictions indicate a plausible mechanism to the apparition of the yield stress. These processes also lead to a nonlinear behavior of the birefringence, which throughout the shear rate range attains lower values than those of the stress. Moreover, at high shear rates, a two-stage variation of the extinction angle is observed in Fig. 3d. Within this range, the stress increases steeply, as observed in Fig. 3b.

The effect of increasing the number of nodes in one chain for first-order kinetics is exposed in Fig. 4. With respect to results shown in Fig. 1 (two chains and one node), the

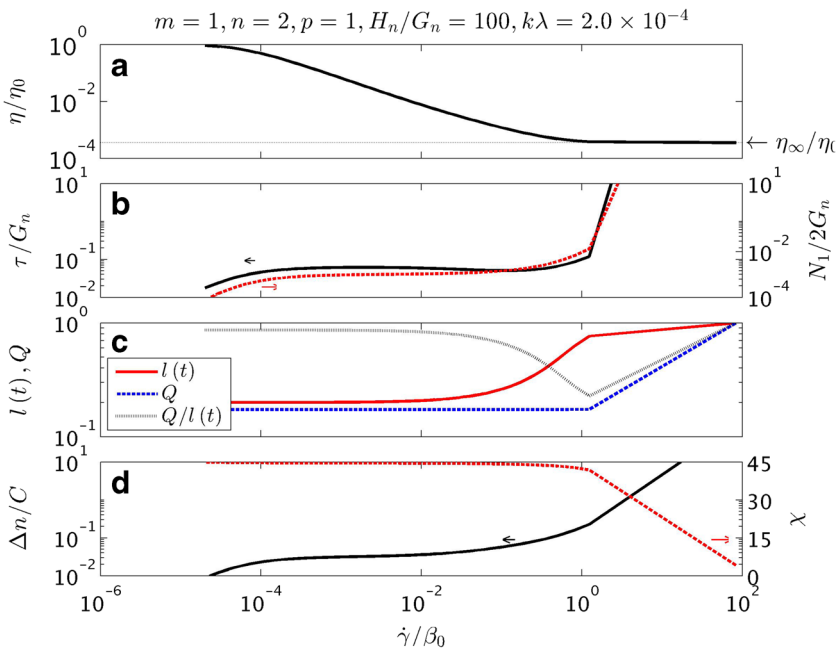

Fig. 4 Same as in Fig. 1, for a system with one chain, two nodes, and first- order kinetic

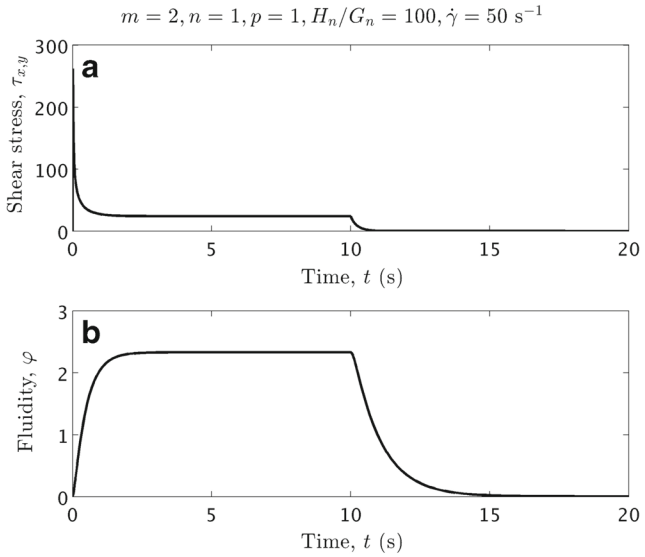

Fig. 5 Same system as in Fig. 1. Applied shear-rate of 50 s^{-1}. Inception of shear flow and relaxation past steady-state. **a** Stress versus time; **b** fluidity versus time

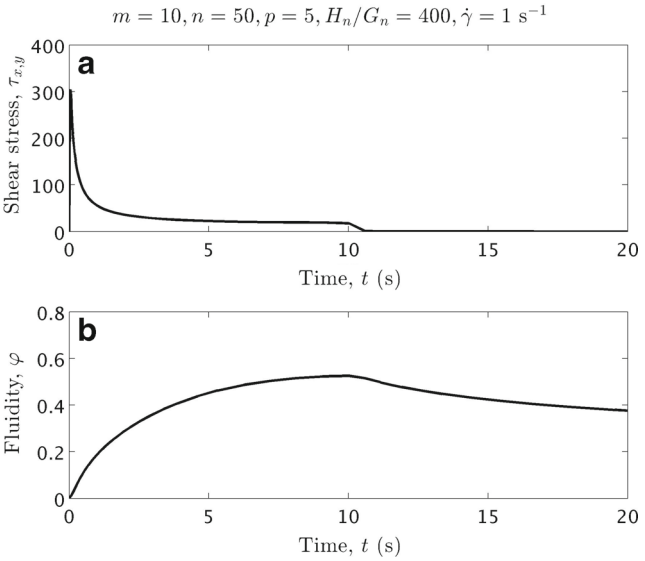

Fig. 7 Same system as in Fig. 3. Applied shear-rate of 50 s^{-1}. Inception of shear flow and relaxation past steady-state. **a** Stress versus time; **b** fluidity versus time

viscosity and stress are modified substantially. A remarkable prediction is the region of negative slope in the stress versus shear-rate curve, in the case of two nodes. The presence of loops and ring structures is known to cause strongly nonlinear effects, in addition to changes in the kinetics due to orientation effects of elastic strains on the loops and rings. The negative slope gives rise to instabilities and eventually shear-banding. This is in contrast to the predicted N_1 curve, which is monotonically increasing function of shear-rate.

Inception of shear flow and stress relaxation

Figures 5, 6, 7 and 8 show predictions of the stress and fluidity at the inception of shear flow, attainment of steady state, and subsequent relaxation as the flow is arrested. Figure 5a, b correspond to a system with two chains and one node with first order kinetics at a shear rate of 50 s^{-1}. The stress shows an initial overshoot at short times and rapidly attains steady state. At time equal to 10 s, the flow is arrested and

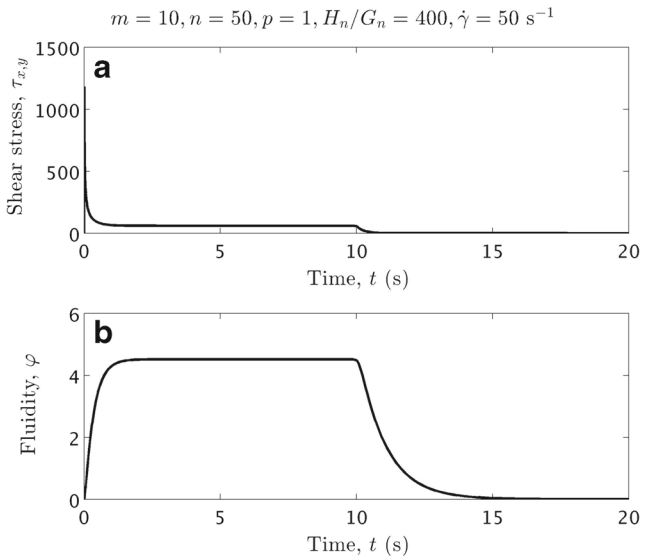

Fig. 6 System with 10 chains, 50 nodes, first-order kinetic and applied shear-rate of 50 s^{-1}. Inception of shear flow and relaxation past steady-state, **a** Stress versus time; **b** fluidity versus time

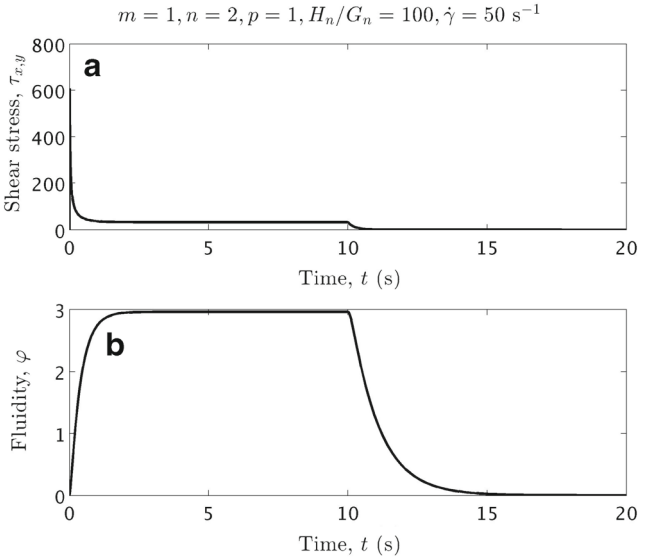

Fig. 8 Same system as in Fig. 4. Applied shear-rate is 50 s^{-1}. Inception of shear flow and relaxation past steady-state. **a** Stress versus time; **b** fluidity versus time

the stress relaxes. The fluidity in turn describes a monotonic increase, a steady state and relaxation with different time scale to that of the stress. These predictions illustrate that the stress relaxation time scale is different to that of the fluidity representing the structure of the system. Although for times longer than 11 s, the stress has already relaxed, the structure is still evolving and recovers at times around 15 s. In other words, structure recovery is achieved at time scales longer than the stress relaxation time.

Figure 6a, b show the effect of increasing the number of chains and nodes for first-order kinetics. An increase in the maximum of the overshoot at short times reveals increased elasticity as compared to results in Fig. 5a. The fluidity in turn increases at steady-state with respect to the previous cases, but relaxes with the same time scale as in Fig. 5b. This result reveals that the structure recovery-time is a strong function of the kinetic order, as clearly shown in Fig. 7a, b. Here, the kinetic order is changed to 5, for a shear rate of 1 s^{-1}. The kinetics in this case induces a dominant reformation function producing large nodes concentration. The stress overshoot is nevertheless large at this small shear rate, depicting increased elasticity. Moreover, the structure recovery time has increased drastically as well as the time to achieve steady-state. The important effect shown here is the large difference exhibited between the stress relaxation time and the structure recovery time. This nonlinear behavior indicates increased elasticity resulting from a dense network.

The effect of increasing the number of nodes or loops within the same chain is analyzed in Fig. 8a, b. Here, the case of first-order kinetics with one chain and two nodes at the shear rate of 50 s^{-1} is considered. With respect to the case shown in Fig. 5 (first-order kinetics with two chains and one node) at the same shear rate, various changes are observed. In the case of two nodes, the overshoot in the stress is larger, more than twice, than that corresponding to the case of one node, revealing increased elasticity. The change in the magnitude of the fluidity reflects profound structure changes as the number of nodes is increased.

Shear thickening

The model analyzed here can predict shear-thickening behavior, in which the fluidity decreases with increasing shear-rate. In turn, the extensibility also decreases as a function of shear rate. Equations 40 and 54 are then modified by setting $\varphi_0 > \varphi_\infty$. Results of the simulations are shown in Figs. 9 and 10.

The nonlinear regime of deformation is attained as the extensibility starts from one at low shear rates and reaches smaller values corresponding to the number of chains and nodes for increasing shear-rate. As the end-to end distance of the segments increases, the nonlinear regime is attained when it reaches values near the extensibility governed by the topology of the network. In a dense network, the rate of decreasing extensibility with shear-rate is large, so the nonlinear regime is found at small end-to-end distances. This behavior intends to mimic the process or mechanism by which the shear-induced structures (SIS) responsible for the shear-thickening are formed.

Figure 9 presents the case of one chain and one node with first-order kinetics. The end-to end distance increases with shear rate up to the point where it meets the extensibility curve, which decreases with shear rate (see Fig. 9c). The

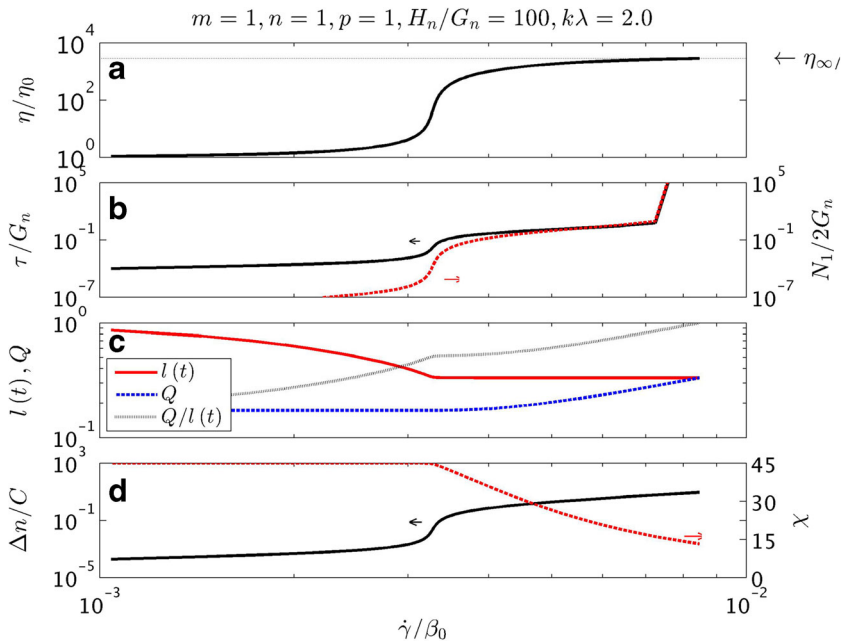

Fig. 9 System with one chain, one node, and first-order kinetics. Rheological functions with nondimensional shear rate with shear-thickening behavior. **a** Normalized viscosity; **b** normalized stress and first normal stress difference; **c** extensibility, end-to-end distance of the segments, and their ratio; and **d** birefringence and extinction angle

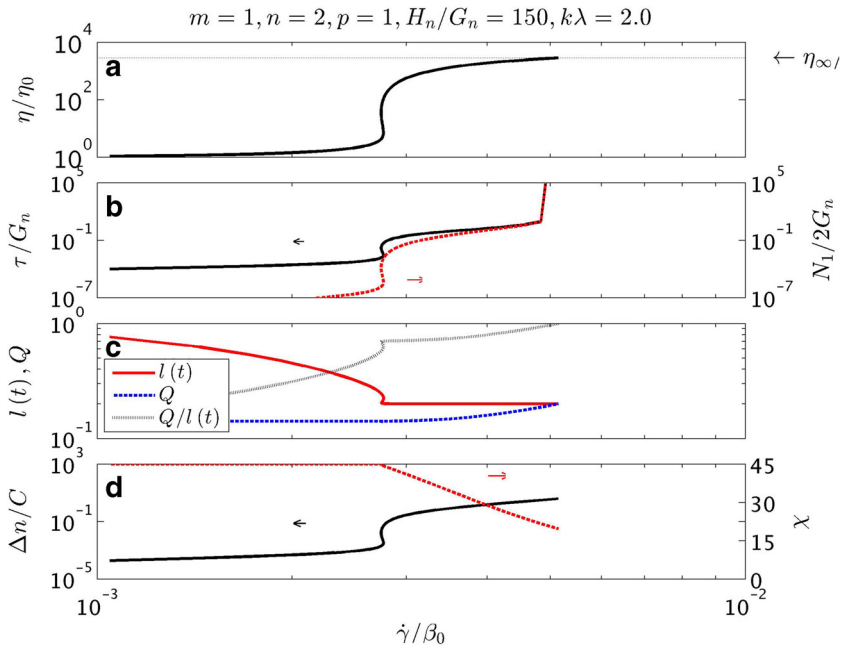

Fig. 10 Same as in Fig. 9 for system with one chain, two nodes, and first-order kinetics

viscosity (Fig. 9a) presents a sudden increase at a critical shear rate and thereafter, for larger shear rates, an asymptotic region is reached, corresponding to an abrupt increase in the stress and first normal stress difference (Fig. 9b), where a two-stage growth in stress and N_1 is predicted. An interesting result is the growth of the birefringence, which is similar to that of the stress at low shear rates.

In Fig. 10, the effect of increasing the number of nodes in a single chain is exposed. A qualitatively different pattern emerges: the viscosity in Fig. 10a presents a reentrant region (or multi-valued region) within an interval in shear rates, ascribed to a multi-valued extensibility (Fig. 10c). The stress and first-normal stress difference (Fig. 10b) also present the reentrant region, followed by another sudden increase at relatively larger shear rates. A most interesting result is the birefringence variation with shear rate, wherein it is known that in which the multi-valued region generates hysteresis cycles in the conformation of the molecular segments. These results are in agreement with predictions of a conformation-dependent dumbbell model, wherein a sudden increase in the molecular conformation at a critical shear rate is observed as the shear-rate increases. The decreasing shear rate path follows a different trajectory, preserving the molecular deformation for lower values than the critical shear rate.

Interrupted shear

In this shear history, initially, the shear stress displays an overshoot at the inception of shear flow, and then it attains steady state at longer times. Then, the flow is interrupted and the stress relaxes with time. After a rest period, the same shear rate is applied and a second overshoot is observed. When the rest period is long enough for the recovery of the initial structure, the second overshoot has a similar magnitude of the first one; however, when the rest period is short, the magnitude of the second overshoot may be smaller than that of the first one.

Since the rest period may be associated with the time for structure rebuilding, when the rest period is sufficiently long, structure rebuilding is complete, and the material recovers its initial structure. But when the rest period is

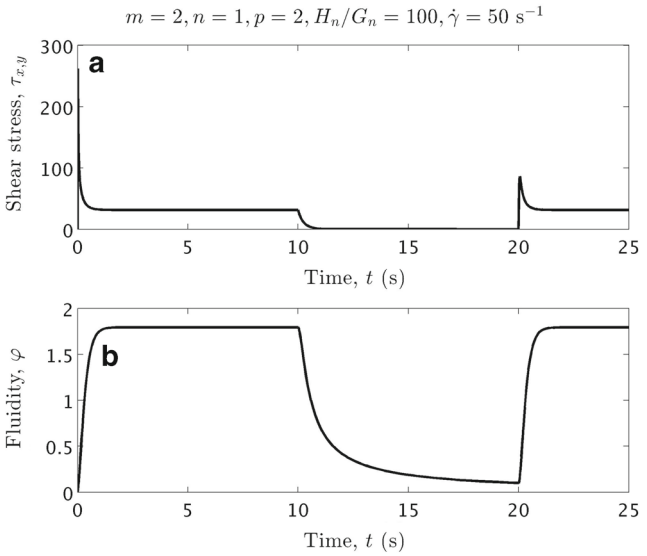

Fig. 11 Same system as in Fig. 2 and shear rate of 50 s^{-1}. Inception of shear flow and interrupted shear predictions: **a** stress versus time; **b** fluidity versus time

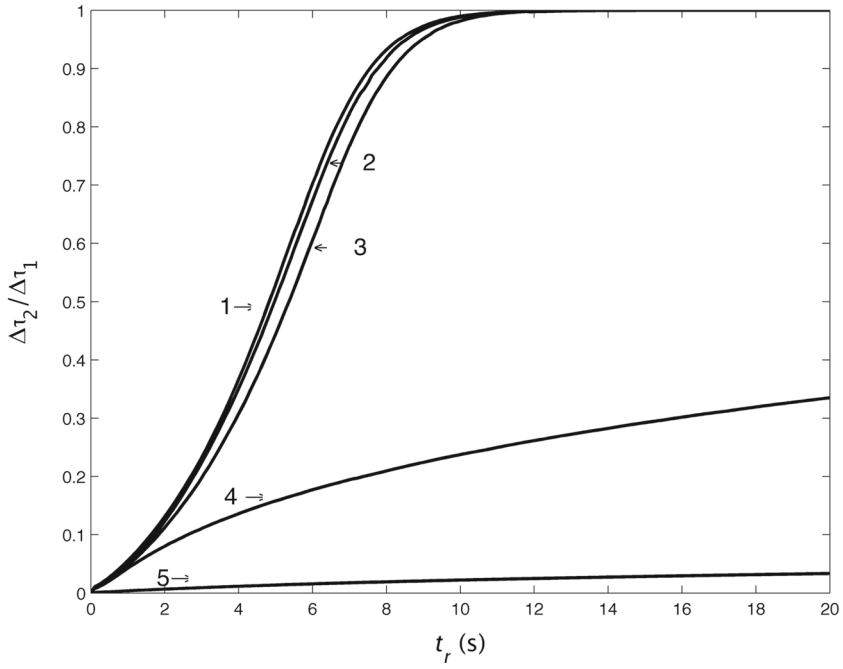

Fig. 12 Interrupted shear predictions. Ratio of magnitudes of the second overshoot divided by the first overshoot versus rest time between overshoots. Curve 1-case 1 (Fig. 5), curve 2-case 5 (Fig. 11), curve 3-case 3 (Fig. 8), curve 4-case 2 (Fig. 6), and curve 5-case 4 (Fig. 7). Corresponding to those presented in Figs. 5 to 8 and 11, respectively

short, structure rebuilding is not complete, and the magnitude of the overshoot is smaller, reflecting the presence of another structure.

Figure 11a, b illustrate predictions of interrupted shear of the stress and fluidity as a function of time for two chains, one node, kinetic order 2, and shear-rate of 50 s^{-1}. In this case, (Eq. 54 is now quadratic), the reformation rate of the structure increases with consequent increase in the node formation. Although the stress fully relaxes as exhibited in Fig. 11a, the fluidity has not relaxed during the stress relaxation time scale (Fig. 11b). Predictions clearly illustrate that during the relaxation time of the stress, the structure has not recovered and consequently the second stress overshoot is smaller than the first one.

Figure 12 depicts a series of predictions of the overshoot ratio (magnitude of the second overshoot divided by the magnitude of the first overshoot) varying the rest time between arrest and inception of flow. Cases 1 to 5 correspond to those analyzed in Figs. 5 to 8 and Fig. 11. Cases 1 and 3 have same kinetic order and shear rate, but different number of chains and nodes. They show basically the same behavior, in which the second overshoot attains the magnitude of the first overshoot when the rest time is longer than 8 s. Case 2 corresponds to a change in the number of chains and nodes with respect to case 1. The recovery of the structure in this case is very slow, and the overshoot ratio in this case is around 0.6 after 20 s of rest time. In this context, case 4 represents the extreme case where no recovery is evidenced after 20 s of rest time (the kinetic order is 5 at 1 s^{-1} of shear-rate). Case 5 corresponds to the system with two nodes. Curves corresponding to kinetic order of two comply with experimental data of 0.11 M CTAT aqueous solution (Puig et al. 2004).

The difference in time scales of stress relaxation and recovery time evidences the general behavior of thixotropic materials. These time-dependent phenomena are clearly predicted by the model presented here.

Concluding remarks

A nonlinear viscoelastic model based in the transient network formulation of constitutive equations containing simplified kinetics is presented in this analysis. To account for variable entanglement density in the flow domain observed in complex systems, various microstates are defined, representing several scenarios of molecular interactions. Particular cases are treated, from microstates containing free chains to more entangled microstates containing more nodes. The evolution of the microstates is represented by a set of coupled, time-dependent kinetic equations, in which the detailed kinetics are substituted by a global kinetics involving a reduced number of microstates. Depending upon the flow characteristics, the concentration of microstates at a certain time defines the extensibility (maximum segment length) of the segments forming the network. The rheological functions (shear and normal stresses, birefringence) calculated from the classical expressions of the transient network formulation are then functions of the dynamics of the microstates. It is shown that in particular cases for

specific kinetics, the model is consistent with phenomenological models containing a description of the kinetics of breakage-reformation of the system structure.

The global kinetics considered here embodies several particular cases. For the particular case of $p = 2$ and $m = 2$ in Eqs. 21 and 22, the kinetics of the two species model of Vasquez et al. (2007) is recovered. The kinetics analyzed here is therefore more general, including predictions such as the behavior of time-dependent thixotropic materials.

This approach considers the rigorous description of the moment equations derived from the well-established kinetic theory for nonhomogeneous flows (Bhave et al. 1991). In the particular case of no diffusion and considering further a nonlinear spring force with variable extensibility (which is itself a function of the kinetic process), the expressions for the stress components and optical variables are similar to those of Rincón et al. (2005), with added microstates. This framework thus provides a link between the previous model by Rincon and the present approach, which is in agreement with predictions and experiments exposed in Rincon paper. However, the present approach allows for a framework to include other microstates (loops or rings, etc.) based on the concept of a representative variable for the system internal-structure, in this case, the fluidity. One of the novel features exposed here is the explicit balance of the stress relaxation time as compared to the structure relaxation time represented by the fluidity. The structure relaxation time difference with that of the stress allows for a variety of time-dependent predictions, including thixotropy. With regard to the loop structures, Cates and Fielding (2007) have pointed out that these structures cause strongly nonlinear effects, in addition to changes in the kinetics due to orientation effects of elastic strains on the loops and rings. Phenomena such as shear-thickening may be explained on the basis of this nonlinear response. We have considered predictions of various nodes in the calculations, with results that show a remarkable prediction of the multi-valued region of the stress against shear-rate, wherein a maximum in the stress is predicted with a negative slope of the flow curve (see Fig. 4).

Comparison with experiments is provided in the manuscript, although the experimental data are not reproduced here. Indeed, curves corresponding to cases 1–3 in Fig. 12 are in agreement with experimental data of 0.11M CTAT aqueous solution (Puig et al. 2004). To better demonstrate this concordance, data and predictions are illustrated. In addition, other references are considered, such as the paper by Stratton and Butcher on polymer solutions (Stratton and Butcher 1973, see their Fig. 4), wherein the maximum stress from stop-start experiments against rest-time is plotted. This curve is in remarkable agreement with predictions shown in Fig. 12 (cases 1–3) of this work.

Moreover, in polypropylene/clay hybrid materials, Solomon et al. (2001) clearly illustrate the dependence of the stress overshoot on the rest time, as an indication that the structure of the material evolves, even under quiescent conditions (when the stress has already relaxed). The experimental curves disclosed for this system are also in remarkable agreement with predictions of Fig. 12. To our knowledge, very few models are able to predict this behavior in such extent.

One of the models derived from kinetic theory which is similar in some aspects to the present model is the FENE-CR (Chilcott and Rallison 1988). This model possesses nonlinear spring force and variable extensibility (the extensibility level is fixed as an input value). The first normal-stress difference presents highly nonlinear variation with the shear-rate; deviations from the slope of 2 (Oldroyd-B behavior) augment as the extensibility decreases. In the present model, the extensibility is a function of the kinetic process, but depending upon the structures formed at low shear rates (loops, etc.), the extensibility evolves with time and shear rate. In the case of loops, the extensibility is small and hence a highly nonlinear response is expected at low shear-rates.

Models predicting strain-hardening properties comply with a microstructure with limited extensibility. Indeed, in the original Doi and Edwards (D-E) tube concept of polymer chain reptation, caused by a mesh of constraints that confines the chain laterally to a tube-like region, the tension of the deformed macromolecular chain remains constant and equal to its equilibrium value. Consequently, the original D-E model does not account for strain-hardening, notably under extensional flow. However, it is experimentally observed that the tension in the molecular chains increases with an increase in deformation. Wagner et al. have modified the D-E model by introducing the molecular stress function (Wagner et al. 2001) to account for strain-hardening. Long-chain branched polymers show enhanced strain-hardening, consistent with decreased extensibility as loops and other microstructures may likely be formed in the quiescent state. The nonlinear behavior of our model in the low shear-rate range (notably the shear-thickening results) reflects the behavior of strain-hardening systems and predictions should be similar to those of modified tube models. The reentrant viscosity curve (Fig. 10a) resembles experimental results exposed in the current literature on shear-thickening fluids (Hu et al. (1998), see Fig. 2).

Finally, the perspective of this work should naturally include the diffusion terms that have been neglected in the present approach. We have considered the case where the diffusion term for the concentrations in Eqs. 15 and 16 is included and, in fact, the numerical scheme converges more rapidly, giving rise to smoother transitions in the rheological predictions. But the more general approach is that of

solving the Fokker-Planck equations (11) and (12) and work out the statistical averages without Peterlin pre-averaging. This approach will render a solution to the diffusive case in a more consistent manner (Kroger 2008).

Acknowledgments Financial support from project CONACYT-219810 is gratefully acknowledged.

References

Bautista F, Soltero J, Prez-Lpez J, Puig J, Manero O (2000) On the shear banding flow of elongated micellar solutions. J Non-Newtonian Fluid Mech 94(1):57–66. doi:10.1016/s0377-0257(00)00128-2

Bautista F, Soltero JFA, Macías ER, Puig JE, Manero O (2002) Irreversible thermodynamics approach and modeling of shear-banding flow of wormlike micelles. J Phys Chem B 106:13018–13026

Beris AN, Mavrantzas VG (1994) On the compatibility between various macroscopic formalisms for the concentration and flow of dilute polymer solutions. J Rheol 38(5):1235. doi:10.1122/1.550541

Bhave AV, Armstrong RC, Brown RA (1991) Kinetic theory and rheology of dilute, nonhomogeneous polymer solutions. J Chem Phys 95(4):2988. doi:10.1063/1.460900

Bird RB, Curtiss CF, Armstrong RC, Hassager O (1987) Dynamics of Polymeric Liquids, Kinetic Theory, vol 2, 2nd edn. Wiley-Interscience

Caram Y, Bautista F, Puig JE, Manero O (2006) On the rheological modeling of associative polymers. Rheologica Acta 46(1):45–57. doi:10.1007/s00397-005-0066-y

Cates M, Fielding S (2007) Giant Micelles. Properties and Applications, Surfactant Science Series, vol 140. CRC Press Taylor & Francis, USA

Chilcott M, Rallison J (1988) Creeping flow of dilute polymer solutions past cylinders and spheres. J Non-Newtonian Fluid Mech 29:381–432. doi:10.1016/0377-0257(88)85062-6

Green MS, Tobolsky AV (1946) A new approach to the theory of relaxing polymeric media. J Chem Phys 14(2):80. doi:10.1063/1.1724109

Hu YT, Boltenhagen P, Pine DJ (1998) Shear thickening in low-concentration solutions of wormlike micelles. I. direct visualization of transient behavior and phase transitions. J Rheol 42(5):1185. doi:10.1122/1.550926

Kroger M (2008) Consistent closure schemes for statistical models of anisotropic fluids. J Non-Newtonian Fluid Mech 149(1-3):40–55. doi:10.1016/j.jnnfm.2007.05.007

Lodge AS (1956) A network theory of flow birefringence and stress in concentrated polymer solutions. Trans Faraday Soc 52:120. doi:10.1039/tf9565200120

Manero O, Bautista F, Soltero J, Puig J (2002) Dynamics of worm-like micelles: the cox-merz rule. J Non-Newtonian Fluid Mech 106(1):1–15. doi:10.1016/s0377-0257(02)00082-4

Puig JE, Escalante J, Macas E, Soltero JFA, Bautista F, Manero O (2004) Recent research developments in surfaces and colloids, vol 1, Research Signpost, chap On the shear-banding flow and electrostatic interactions in polymer-like micellar solutions, pp 145–167

Rincón E, Chávez A, Herrera R, Manero O (2005) Rheological modelling of complex fluids: a transient network model with microstates. J. Non-Newtonian Fluid Mech 131(1-3):64–77. doi:10.1016/j.jnnfm.2005.08.011

Solomon MJ, Almusallam AS, Seefeldt KF, Somwangthanaroj A, Varadan P (2001) Rheology of polypropylene/clay hybrid materials. Macromolecules 34(6):1864–1872. doi:10.1021/ma001122e

Soltero JFA, Bautista F, Puig JE, Manero O (1999) Rheology of cetyltrimethylammonium p-toluenesulfonate-water system 3. Nonlinear viscoelasticity. Langmuir 15(5):1604–1612. doi:10.1021/la971299a

Stratton RA, Butcher AF (1973) Stress relaxation upon cessation of steady flow and the overshoot effect of polymer solutions. J Polym Sci Polym Phys 11(9):1747–1758. doi:10.1002/pol.1973.180110907

Vaccaro A, Marrucci G (2000) A model for the nonlinear rheology of associating polymers. J Non-Newtonian Fluid Mech 92(2-3):261–273. doi:10.1016/s0377-0257(00)00095-1

Vasquez PA, McKinley GH, Cook LP (2007) A network scission model for wormlike micellar solutions. J Non-Newtonian Fluid Mech 144(2-3):122–139. doi:10.1016/j.jnnfm.2007.03.007

Wagner MH, Rubio P, Bastian H (2001) The molecular stress function model for polydisperse polymer melts with dissipative convective constraint release. J Rheol 45(6):1387. doi:10.1122/1.1413503

Warner HR (1972) Kinetic theory and rheology of dilute suspensions of finitely extendible dumbbells. Ind Eng Chem Fundamentals 11(3):379–387. doi:10.1021/i160043a017

Weston R, Schwarz H (1972) Chemical Kinetics. Fundamental topics in physical chemistry, Prentice Hall

Yamamoto M (1958) The visco-elastic properties of network structure III. normal stress effect (weissenberg effect). J Phys Soc Jpn 13(10):1200–1211. doi:10.1143/jpsj.13.1200